analytical chemistry

pubs.acs.org/ac Article

Multiregion Linear DNA Walker-Mediated Ultrasensitive Electrochemical Biosensor for miRNA Detection

Tong-Lin Hou, Liang Zhu, Xiao-Long Zhang, Ya-Qin Chai, and Ruo Yuan*

Cite This: *Anal. Chem.* 2022, 94, 10524−10530 Read Online

ACCESS | Metrics & More | Article Recommendations | Supporting Information

ABSTRACT: In this work, an intelligent multiregion linear DNA walker (MLDW) with a high walking rate and a high amplification efficiency was explored for ultrasensitive detection of miRNA. Significantly, amounts of functional domain could be concentrated in a long linear DNA obtained by the target miRNA-mediated rolling-circle amplification to simultaneously increase the local concentration and collision probability, resulting in an obviously improved reaction rate. Impressively, the MLDW can accomplish the reaction within 30 min, which is at least 4 times beyond that of traditional single-leg and multiple-leg DNA walkers. As a proof of concept, the high-efficiency MLDW was used to develop an electrochemical biosensing platform for ultrasensitive detection of target miRNA-21 with a low detection limit down to 36 aM. Therefore, the MLDW we designed puts forward an innovative insight to construct a functional DNA nanodevice and promote the investigation of the inherent performance of nucleic acid signal amplification for ultimate application in the detection of biomolecules and clinical disease diagnosis.

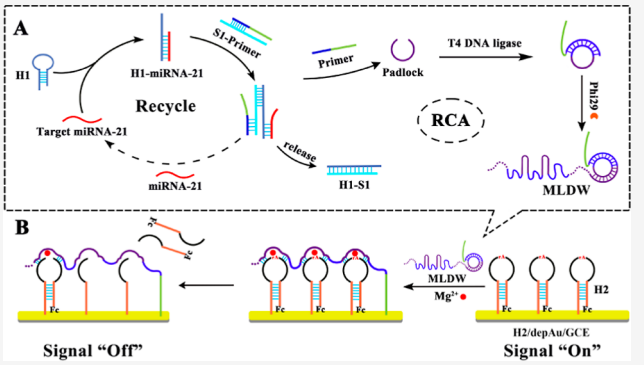

INTRODUCTION

Because MicroRNA (miRNA) is a kind of low-expression single-stranded RNA and plays an essential role in cancer development, its sensitive detection is of great importance.[1−5] Because of the low abundance of miRNA in cancer cells, a number of signal amplification methods such as northern blotting, quantitative reverse transcription polymerase chain reaction (qRT-PCR), and microarray analysis have been developed to achieve sensitive detection of miRNA.[6−11] However, limited by the disadvantages of complicated operation, high cost, and high environmental disturbance, these methods cannot meet the requirements of improved universality. Therefore, it is essential to develop a novel nucleic acid signal amplification method with higher efficiency for ultrasensitive miRNA detection.

DNA walkers, a kind of autonomous molecular nanomachines, are considered an attractive nucleic acid amplification strategy due to the ability of the cascade signal improvement generated by their autonomous movement.[12−19] According to the nanostructure, DNA walkers can be divided into single-leg DNA walkers[20,21] and multiple-leg DNA walkers.[22−25] Single-leg DNA walkers possess the advantage of low steric hindrance and simple construction;[26] however, they suffer from poor functional domains leading to a low walking efficiency. Multiple-leg DNA walkers increase the local concentration of the functional domain, resulting in an increased walking efficiency to some extent. Nevertheless, the increased steric hindrance and the contractible reaction space of traditional multiple-leg DNA walkers hinder further improvement of their walking efficiency.[27−29] Therefore, it remains a challenge to develop a simple DNA walker with low steric hindrance and abundant functional domains for obtaining a high walking efficiency. On the other hand, according to the walking style, the DNA walkers can also be divided into free-type[30,31] and anchor-type,[32,33] and compared with the free-type walker, the anchor-type walker has a better continuously walking ability and a higher walking efficiency.[34,35] Thus, to address the challenge of low walking efficiency in traditional single-leg and multiple-leg DNA walkers, it is expected to achieve significant improvement in walking efficiency by developing an anchor-type single-leg walker with multiple functional domains, small steric hindrance, and a large reaction space.

In this work, we design a versatile multiregion linear DNA walker (MLDW) as an anchor-type single-leg walker with multiple functional domains, small steric hindrance, and a large reaction space and applied it to construct an ultrasensitive electrochemical biosensor for the rapid detection of miRNA.

Received: May 7, 2022
Accepted: July 1, 2022
Published: July 13, 2022

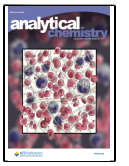

https://doi.org/10.1021/acs.analchem.2c02004
Anal. Chem. 2022, 94, 10524−10530

Scheme 1. (A) Schematic Illustration of the Development of the (MLDW) via Target miRNA-21-Mediated RCA; (B) Illustration of the Electrochemical-Biosensing Platform Construction via the MLDW for miRNA Detection

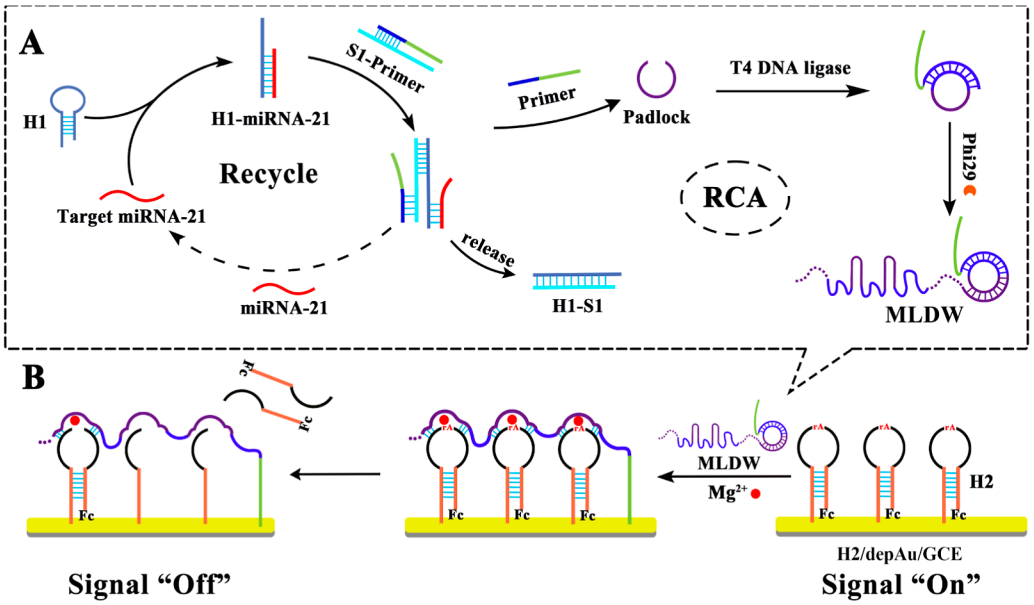

As displayed in Scheme 1, once the target miRNA-21 opens the hairpin H1 to form the duplex H1-miRNA-21 with the prelocked toehold exposed, the duplex S1-primer could hybridize further with the duplex H1-miRNA-21 to release the miRNA-21 and primer simultaneously, and the released miRNA-21 could participate in the next reaction and output amounts of primer. Subsequently, with the assistance of padlock, T4 DNA ligase, Phi29 DNA polymerase, and dNTP, the rolling circle amplification (RCA) could be activated by the primer and output lots of MLDWs. Finally, when the MLDW was immobilized on the electrode which was modified with DNA H2 via the polyA-Au,[36,37] it can walk on the electrode surface, and the DNAzyme could cleave a specific RNA phosphodiester linkage in the H2 with the help of Mg^{2+} accompanied with the release of Fc from the surface and the variation of the electrochemical signal response, thus realizing the sensitive detection of miRNA-21. As a result, based on the high-efficiency MLDW and nucleic acid signal amplification, the developed electrochemical biosensing platform could realize the rapid and ultrasensitive detection of miRNA-21. Therefore, the intelligent MLDW gives an unique insight to study nucleic acid signal amplification and possesses potential for application in biomarker analysis and disease diagnostics.

EXPERIMENTAL SECTION

Construction of the Electrochemical Biosensor. The glass carbon electrode (GCE) was finely polished with 0.3 μm alumina slurry and rinsed with distilled water. The electrode surface was coated with gold particles (depAu) through electrodepositing in $HAuCl_4$ for 30 s (−0.2 V). Then, 10 μL of Tris−HCl (pH 7.4) containing annealed hairpin H2 (2 μM) was dripped onto the electrode surface (depAu/GCE) and kept at room temperature overnight. At last, the modified electrode was completely rinsed with distilled water to remove non-specific adsorbed DNA on the surface.

Preparation of the MLDW. First, the hairpin H1 was annealed to form a stable hairpin structure. Then, 15 μL of hairpin H1 (2 μM), 2.5 μL of target miRNA-21 with different concentrations, and 2.5 μL of S1 (10 μM) and primer (2.5 μL 10 μM), respectively, were mixed and reacted for 3 h to achieve the full hybridization reaction. Then, 2.5 μL of padlock (10 μM), 10× T4 DNA ligase buffer (3 μL) and 2 μL of T4 DNA ligase (5 U/μL) were mixed with the solutions to react at 37 °C (4 h) for obtaining the circle padlock. Subsequently, the solution (30 μL) was heated (10 min, 65 °C) for the inactivation of the T4 DNA ligase. Next, dNTP (5 μL, 25 mM), 10× Phi29 DNA polymerase buffer (4 μL), and Phi29 DNA polymerase (1 μL, 10 U/μL) were mixed with the above solutions and reacted (37 °C, 30 min) to form the MLDW. Finally, the reaction mixture containing MLDW was heated (10 min, 65 °C) to denature the Phi29 DNA polymerase, and the prepared MLDW was stored (4 °C) for follow-up experiments.

Polyacrylamide Gel Electrophoresis. First, 40% acrylamide (10 mL), distilled water (10 mL), 5× TBE buffer (5 mL), 10% APS (200 μL), and TEMED (15 μL) were mixed successively under constant stirring. Following that, different DNA reaction solutions were mixed with the DNA-loading buffer (6×), then polyacrylamide-gel electrophoresis (PAGE) was used to characterize the DNA samples in 1× TBE buffer at 30 mA for 30 min (16%, pH = 8.0).

RESULTS AND DISCUSSION

Characterization of MLDW. We used atomic force microscopy (AFM) to study the morphology of MLDW. As shown by the results displayed in Figure 1, an evident linear DNA nanostructure could be easily observed, demonstrating the successful operation of MLDW via RCA.

PAGE Analysis. The formation of MLDW and the cleaving process of DNAzyme were proved by gel electrophoresis. As the results illustrated in Figure 2A, the obvious bands in lanes 1−6 are related to miRNA-21, H1, S1, padlock, primer, and H2, respectively. After the H1 was added into the miRNA-21 solution (lane 7), we could notice an obvious band with decreased electrophoretic mobility (the top band in lane 7) compared with lane 1 (miRNA-21) and lane 2 (H1), successfully demonstrating the hybridization of H1 and miRNA-21. When the S1 was mixed with the primer, a

https://doi.org/10.1021/acs.analchem.2c02004
Anal. Chem. 2022, 94, 10524−10530

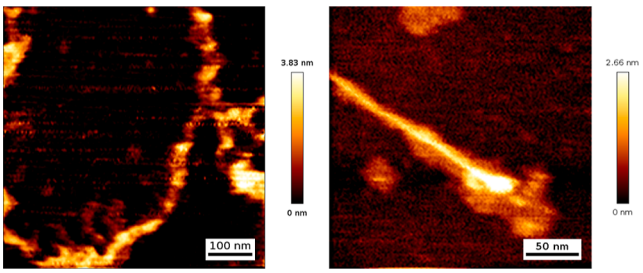

Figure 1. AFM images of MLDW (scale bars: 100 nm and 50 nm).

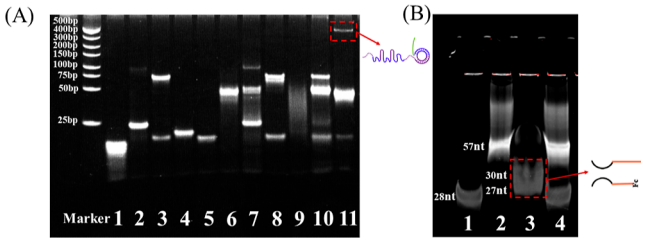

Figure 2. PAGE characterization analysis of (A) the formation of MLDW: lanes 1−6: miRNA-21 (4 μM), H1 (1 μM), S1 (1 μM), padlock (1 μM), primer (1 μM), and H2 (1 μM); lane 7, miRNA-21 (1 μM) + H1 (1 μM); lane 8, S1 (1 μM) + primer (1 μM); lane 9, padlock (1 μM) + primer (1 μM); lane 10, miRNA-21 (1 μM) + H1 (1 μM) + S1 (1 μM) + primer (1 μM); lane 11, miRNA-21 (9 nM) + H1 (1 μM) + S1 (1 μM) + primer (1 μM) + padlock (1 μM) (in the presence of Phi29 DNA polymerase, T4 DNA ligase, and dNTPs) (PAGE 16%, 30 mA, 30 min) and (B) cleaving process of DNAzyme: lane 1, DNAzyme (2 μM); lane 2, H2 (2 μM); lane 3, DNAzyme (2 μM) + H2 (2 μM) (with the Mg^{2+} of 100 mM); and lane 4, DNAzyme (2 μM) + H2 (2 μM) (without Mg^{2+}). nt: nucleotide, bp: base pair.

brighter band with slow mobility corresponding to the duplex S1-primer was present (lane 8), demonstrating the successful hybridization between them. In addition, a band with quite slower migration (lane 9) appeared after padlock was mixed with the primer, verifying that the primer could react with padlock. After the miRNA-21 and H1 were mixed the mixture of S1 and primer, a band (the top band in lane 10) corresponding to duplex S1−H1 could be observed, indicating the successful proceeding of the nucleic acid signal amplification. Finally, after the miRNA-21, H1, S1, primer, T4 DNA ligase, padlock, Phi29 DNA polymerase, and dNTPs were mixed, an obvious band with low mobility in lane 11 corresponding to the MLDW could be noticed, illustrating that the MLDW was successfully prepared. Moreover, as illustrated in Figure 2B, lane 1 and lane 2 correspond to the DNA strands of DNAzyme and hairpin H2, respectively. Next, with the assistance of Mg^{2+}, H2 was mixed with DNAzyme, and a new band corresponding to DNA strand released from the hairpin H2 could be noticed (lane 3). In comparison, after the hairpin H2 was added to the solution of DNAzyme without the presence of Mg^{2+}, there were only two obvious bands corresponding to H2 and DNAzyme (lane 4), respectively. The results further suggested that the H2 could only be cleaved by the DNAzyme with the help of Mg^{2+}.

Optimization of the Reaction Conditions of MLDW. To realize the optimum performance of this proposed biosensing platform, the reaction time of MLDW preparation and the walking progress of MLDW were optimized, respectively. First, the influence of the reaction time of MLDW preparation was studied. As depicted in Figure 3A, the electrochemical signal responses decreased gradually as the reaction time increased and reached a stationary phase after 0.5 h. Consequently, the optimum reaction time of MLDW preparation was fixed at 0.5 h. Meanwhile, the effect of the walking time of MLDW on the current response of the biosensor was also investigated. As shown in Figure 3B, the current signal of the biosensor decreased as the reaction time increased and reached a plateau after 0.5 h. Therefore, 0.5 h was selected as the optimum walking time of MLDC.

Reaction Rate Comparison of the MLDW with Other DNA Walkers. To demonstrate the excellent efficiency of the MLDW, typical kinetic data of the MLDW were measured, and some different conventional DNA walkers (a, MLDW; b, free-type MLDW; c, anchor-type single-leg DNA walker; and d, free-type single-leg DNA walker) were set as control groups. As shown in Figure 4A, the current feedback of the biosensing platform based on MLDW decreased much faster than those of the biosensing platform based on traditional DNA walkers, demonstrating the superior cleavage efficiency of MLDW.

To further study the kinetic characteristics of the proposed methods, we calculated the corresponding reaction rate in electrochemistry, and as depicted in Figure 4B the initial reaction rate of MLDW (−14.2 μA h^{-1}) is obviously faster than those of free-type MLDW (−8.87 μA h^{-1}), anchor-type single-leg DNA walker (−8.87 μA h^{-1}), and free-type single-leg DNA walker (−5.97 μA h^{-1}). When the variation of the current intensity is close to 0, the MLDW reached equilibrium with the corresponding reaction time of 30 min, which is quite shorter than those of control groups (free-A MLDW: 60 min, free-A single-leg DNA walker: 120 min), and the comparison

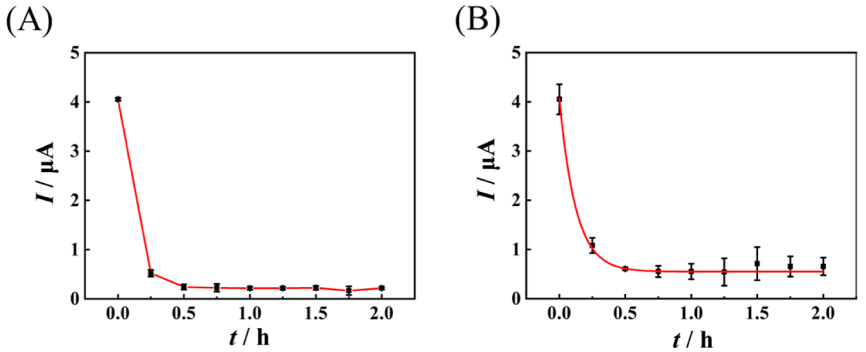

Figure 3. Effects of the reaction time of (A) MLDW preparation and (B) the walking progress of MLDW on the current response of the electrochemical biosensor (the concentration of miRNA-21 is 1 nM, error bars, SD, n = 3).

https://doi.org/10.1021/acs.analchem.2c02004
Anal. Chem. 2022, 94, 10524−10530

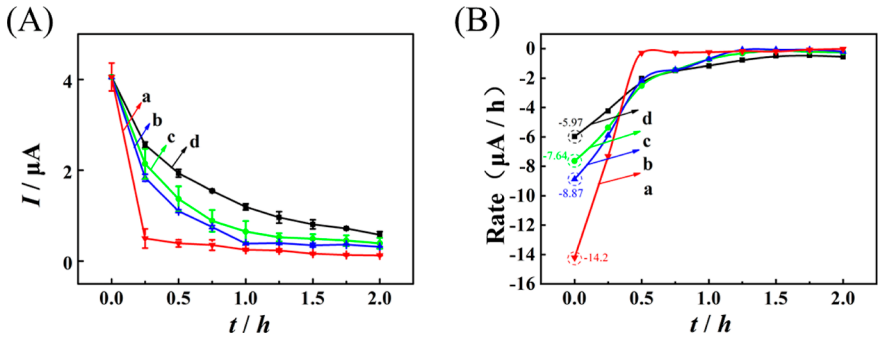

Figure 4. (A) SWV responses of the biosensing platform based on different DNA walkers with 1 nM miRNA-21; (B) reaction rate of different walkers [(a) MLDW, (b) free-type MLDW, (c) anchor-type single-leg walker, and (d) free-type single-leg walker] (error bars, SD, n = 3).

results are listed in Table 1. Moreover, we also compared the reaction time of the MLDW with those of other typical DNA walkers. As shown by the results listed in Table 2, the MLDW has the shortest reaction time. These results above illustrated that the MLDW in this work broke the bottleneck of these conventional nucleic acid amplification methods successfully: low efficiency and long reaction time, making it more promising for application in rapid detection of biomarkers.

Table 1. Comparison of the Developed MLDW with Other Typical DNA Walkers

DNA walker	walking time (h)	reaction rate (μA h^{-1})
free-type single-leg walker	2	−5.97
anchor-type single-leg walker	1.25	−7.64
free-type MLDW	1	−8.87
MLDW	0.5	−14.2

Table 2. Comparison of Recent DNA Walker-Based Efficiency for miRNA Detection

DNA walker	walking time (h)	refs
one-Step DNA walker	4	38
light-actuated 3D DNA walker	3	39
1-assisted DNA walker	4	40
DNAzyme walker	4	41
bipedal DNA walker	2	42
3D DNA walking machines	2	43
DNAzyme walker	2.5	44
3D DNA walker	2	45
enzyme-driven single-leg walker	2	46
MLDW	0.5	this work

Performance Analysis of the Electrochemical Biosensor. As a proof of concept, the high-efficiency MLDW was used to construct an electrochemical biosensor for the rapid and ultrahigh-sensitive detection of miRNA-21. After the reaction conditions were optimized, the current response of the developed electrochemical biosensor to the target miRNA-21 was evaluated by SWV. As we can see, the peak value of SWV decreased with the elevated target concentration (100 aM−10 nM) (Figure 5A), and a good linear relationship between the peak currents and the logarithm of the miRNA-21 concentration could be observed in Figure 5B. The corresponding regression equation can be expressed as $I = -0.4026 \lg c - 2.8259$ (I and c represent the current response and the concentration of miRNA-21, respectively, $R = -0.9999$). The corresponding LOD was as low as 36 aM according to the 3σ criterion. Additionally, as exhibited in Table 3, the prepared electrochemical biosensor illustrated a much wider response range and an obvious LOD, which were ascribed to the glorious amplification efficiency of the MLDW.

Investigation of Reproducibility, Selectivity, and Stability. In order to further evaluate the performance of the prepared biosensing platform, the reproducibility, selectivity, and stability of the electrochemical biosensor were studied. First, to check the reproducibility of the electrochemical biosensor, four prepared electrodes with miRNA-21 (100 pM) under the same experimental conditions were monitored. As shown in Figure 6A, the relative standard deviation (RSD) of 6.95% was realized. Otherwise, after 5

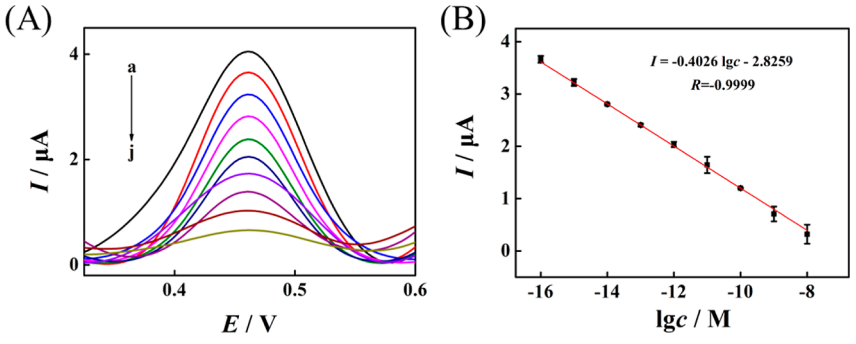

Figure 5. (A) SWV responses of the biosensing system for the target miRNA-21 analysis with different concentrations: (a−j) 0 fM, 100 aM, 1 fM, 10 fM, 100 fM, 1 pM, 10 pM, 100 pM, 1 nM, and 10 nM; (B) calibration curve reflecting the relationship of the SWV peak current vs lg c (error bar, SD, n = 3).

https://doi.org/10.1021/acs.analchem.2c02004
Anal. Chem. 2022, 94, 10524−10530

Table 3. Comparison of this Strategy with Other Studies for Detection of miRNA

analytical methods	linear range	LOD	refs
fluorescence	50 pM to 5 nM	10 pM	47
fluorescence	1 pM to 10 nM	0.35 pM	48
PEC	0.5 fM to 1.0 nM	0.29 fM	49
PEC	1 fM to 1.0 nM	0.33 fM	50
ECL	1 fM to 10 nM	0.33 fM	51
ECL	1 fM to 100 pM	0.18 fM	31
electrochemical	10 fM to 1.0 nM	3.5 fM	52
electrochemical	100 fM to 100 nM	33.6 fM	18
electrochemical	1.0 fM to 1.0 nM	0.28 fM	25
electrochemical	0.2 pM to 2 nM	0.11 pM	33
electrochemical	5 fM to 100 pM	2.2 fM	53
electrochemical	10 fM to 20 nM	10 fM	54
electrochemical	0.1 fM to 100 nM	53 aM	55
electrochemical	100 aM to 10 nM	36 aM	this work

days, some control groups with the same miRNA-21 (100 pM) were also investigated (4 °C), and the RSD was 6.94%, exhibiting a desirable reproducibility of the developed biosensor.

Moreover, to study the selectivity of this electrochemical biosensor, three different miRNA sequences (let-7a, miRNA-155, and miRNA-141) were chosen as interferences. As illustrated in Figure 6B, the current signals of the biosensor without target miRNA-21 were ignorable (miRNA-144, miRNA-155, and let-7a). Oppositely, the current response of the electrochemical biosensor with quite less target miRNA-21 (0.1 nM) was much more obvious. Moreover, the signal responses of the biosensor to the mixture containing target miRNA-21 (0.1 nM) and interference miRNAs (b) were almost conformable with the one of the biosensors in the presence of target miRNA-21 alone. These results indicate the satisfactory selectivity of the constructed electrochemical biosensor.

The stability is the key to its real application, in a complex biomedical environment especially, assessed by continuous scans of the electrochemical biosensing platform 20 times (miRNA-21, 0.1 nM). As revealed in Figure 6C, the corresponding SWV response just changed from 88.2 to 107% with the RSD = 5.86%, indicating the excellent stability of this biosensor.

Practical Applicability of the Electrochemical Biosensor in Cancer Cells. So as to evaluate the feasibility of the electrochemical biosensor for the analysis of miRNA-21 in a complex practical biological matrix, the electrochemical response of the biosensor to the miRNA-21 from lysates of MCF-7 and HeLa cells (human cancer cells) was studied, respectively. As illustrated in Figure 7, the electrochemical signal response increased significantly with the elevated number of MCF-7 cells (101−104), showing the high

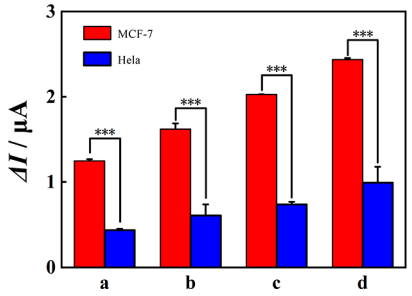

Figure 7. Current response of the developed biosensing platform from cancer cells (HeLa cells and MCF-7 cells) with different numbers: (a) 10^1 cancer cells, (b) 10^2 cancer cells, (c) 10^3 cancer cells, and (d) 10^4 cancer cells (error bars, SD, $n = 3$). *$P < 0.05$, **$P < 0.01$, and ***$P < 0.001$.

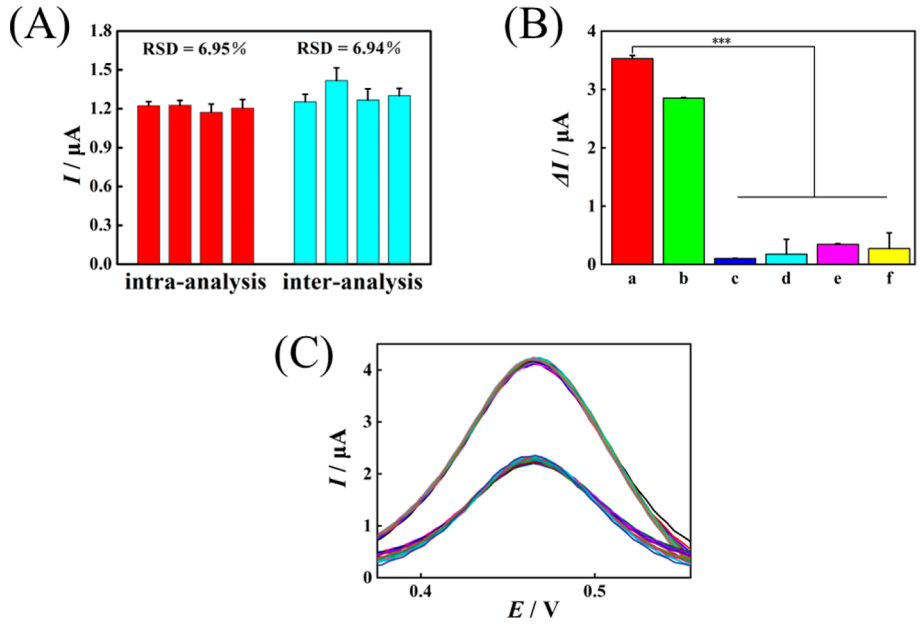

Figure 6. (A) Reproducibility of the prepared biosensing platform (100 pM miRNA-21), error bars, SD, $n = 3$. (B) Selectivity evaluation of the biosensing platform: (a) miRNA-21 (0.1 nM), (b) mixed sample, (c) miRNA-141 (10 nM), (d) miRNA-155(10 nM), (e) let-7a (10 nM), and (f) blank sample (error bars, SD, $n = 3$); and (C) stability detection of the proposed biosensing platform (1 pM miRNA-21, $n = 20$) *$P < 0.05$, **$P < 0.01$, and ***$P < 0.001$.

https://doi.org/10.1021/acs.analchem.2c02004
Anal. Chem. 2022, 94, 10524−10530

expression of miRNA-21 in MCF-7 cells, whereas the current response value was inconspicuous in HeLa cells, suggesting the low expression of miRNA-21 in the HeLa cells. The results were the same as those reported in the literature.[56,57] Therefore, the prepared electrochemical biosensor possessed great potential to monitor the expression of miRNA-21 in cancer cells.

CONCLUSIONS

In summary, we developed an intelligent MLDW with high amplification efficiency to develop an ultrasensitive electrochemical biosensing platform for rapid miRNA-21 analysis. Impressively, the elaborated MLDW not only possessed more functional domain but also faced smaller steric hindrance, exhibiting a superior rate and efficiency compared with those of conventional DNA walkers. Benefiting from these advantages, the MLDW is adopted to successfully construct an ultrasensitive electrochemical biosensor for the rapid detection of miRNA-21, which provides a creative way to develop a potential approach for the functional DNA nanomachine and nucleic acid signal amplification for exploring its applicability and superiority in DNA nanobiotechnology, disease monitoring, and clinical diagnosis.

ASSOCIATED CONTENT

Supporting Information

The Supporting Information is available free of charge at https://pubs.acs.org/doi/10.1021/acs.analchem.2c02004.

Chemicals and materials; apparatus and measurements; cell culture and total RNA extraction; feasibility of the proposed biosensing platform for detection of miRNA; electrochemical characterization of the biosensor; operation of the biosensing platform for the miRNA-21 assay in cancer cell lysates; and calculation of detection limits for miRNA biosensing (PDF)

AUTHOR INFORMATION

Corresponding Author

Ruo Yuan − *Key Laboratory of Luminescence Analysis and Molecular Sensing (Southwest University), Ministry of Education, College of Chemistry and Chemical Engineering, Southwest University, Chongqing 400715, PR China;* orcid.org/0000-0003-3664-6236; Phone: +86 2368252277; Email: yuanruo@swu.edu.cn; Fax: +86 2368253172

Authors

Tong-Lin Hou − *Key Laboratory of Luminescence Analysis and Molecular Sensing (Southwest University), Ministry of Education, College of Chemistry and Chemical Engineering, Southwest University, Chongqing 400715, PR China*

Liang Zhu − *Key Laboratory of Luminescence Analysis and Molecular Sensing (Southwest University), Ministry of Education, College of Chemistry and Chemical Engineering, Southwest University, Chongqing 400715, PR China*

Xiao-Long Zhang − *Key Laboratory of Luminescence Analysis and Molecular Sensing (Southwest University), Ministry of Education, College of Chemistry and Chemical Engineering, Southwest University, Chongqing 400715, PR China*

Ya-Qin Chai − *Key Laboratory of Luminescence Analysis and Molecular Sensing (Southwest University), Ministry of Education, College of Chemistry and Chemical Engineering, Southwest University, Chongqing 400715, PR China;* orcid.org/0000-0003-4392-9592

Complete contact information is available at: https://pubs.acs.org/10.1021/acs.analchem.2c02004

Notes

The authors declare no competing financial interest.

ACKNOWLEDGMENTS

This paper was financially supported by the National Natural Science Foundation of China (22174113, 22176153, and 21974108) and the Fundamental Research Funds for the Central Universities (XDJK2020TY002), China.

REFERENCES

(1) Ambros, V. *Nature* **2004**, *431*, 350−355.
(2) He, P.; Han, W.; Bi, C.; Song, W.; Niu, S.; Zhou, H.; Zhang, X. *ACS Nano* **2021**, *15*, 6961−6976.
(3) Xu, Z.-H.; Gao, H.; Zhang, N.; Zhao, W.; Cheng, Y.-X.; Xu, J.-J.; Chen, H.-Y. *Anal. Chem.* **2021**, *93*, 1686−1692.
(4) Xu, Z.-H.; Wang, H.; Wang, J.; Zhao, W.; Xu, J.-J.; Chen, H.-Y. *Anal. Chem.* **2019**, *91*, 12000−12005.
(5) Xia, L. Y.; Tang, Y. N.; ZhangDong, J. T. N.; Zhou, R. X. *Semin. Cancer Biol.* **2022**, *10*, 1016.
(6) Dong, H.; Lei, J.; Ding, L.; Wen, Y.; Ju, H.; Zhang, X. *Chem. Rev.* **2013**, *113*, 6207−6233.
(7) Dong, J.; Wen, L.; Yang, H.; Zhao, J.; He, C.; Hu, Z.; Peng, L.; Hou, C.; Huo, D. *Anal. Chem.* **2022**, *94*, 5846−5855.
(8) Pritchard, C. C.; Cheng, H. H.; Tewari, M. *Nat. Rev. Genet.* **2012**, *13*, 358−369.
(9) Zhou, M.; Teng, X.; Li, Y.; Deng, R.; Li, J. *Anal. Chem.* **2019**, *91*, 5295−5302.
(10) Chen, Y.; Zhou, S.; Li, L.; Zhu, J.-j. *Nano Today* **2017**, *12*, 98−115.
(11) Zhou, W.; Tian, Y.-F.; Yin, B.-C.; Ye, B.-C. *Anal. Chem.* **2017**, *89*, 6120−6128.
(12) Jung, C.; Allen, P. B.; Ellington, A. D. *Nat. Nanotechnol.* **2015**, *11*, 157−163.
(13) Wang, D.; Vietz, C.; Schröder, T.; Acuna, G.; Lalkens, B.; Tinnefeld, P. *Nano Lett.* **2017**, *17*, 5368−5374.
(14) Lv, S.; Zhang, K.; Zeng, Y.; Tang, D. *Anal. Chem.* **2018**, *90*, 7086−7093.
(15) Lv, S.; Zhang, K.; Zhu, L.; Tang, D. *Anal. Chem.* **2020**, *92*, 1470−1476.
(16) Ji, Y.; Zhang, L.; Zhu, L.; Lei, J.; Wu, J.; Ju, H. *Biosens. Bioelectron.* **2017**, *96*, 201−205.
(17) Zhu, J.; Gan, H.; Wu, J.; Ju, H. *Anal. Chem.* **2018**, *90*, 5503−5508.
(18) Yan, T.; Zhu, L.; Ju, H.; Lei, J. *Anal. Chem.* **2018**, *90*, 14493−14499.
(19) Gan, H.; Wu, J.; Ju, H. *Anal. Chim. Acta* **2019**, *1074*, 142−149.
(20) Oishi, M.; Saito, K. *ACS Nano* **2020**, *14*, 3477−3489.
(21) Xiao, M.; Wang, X.; Li, L.; Pei, H. *Anal. Chem.* **2019**, *91*, 11253−11258.
(22) Chen, A.; Zhuo, Y.; Chai, Y.; Yuan, R. *Chem. Commun.* **2019**, *55*, 13932−13935.
(23) Zhou, R.; Hu, C.; Jin, Y.; Zhang, J.; Du, H.; Yang, P.; Chen, J.; Hou, X.; Cheng, N. *Anal. Chem.* **2020**, *92*, 8909−8916.
(24) Liu, C.; Hu, Y.; Pan, Q.; Yi, J.; Zhang, J.; He, M.; He, M.; Chen, T.; Chu, X. *Biosens. Bioelectron.* **2019**, *136*, 31−37.
(25) Wang, S.; Ji, Y.; Fu, H.; Ju, H.; Lei, J. *Analyst* **2019**, *144*, 691−697.
(26) Lin, M.; Wang, J.; Zhou, G.; Wang, J.; Wu, N.; Lu, J.; Gao, J.; Chen, X.; Shi, J.; Zuo, X.; Fan, C. *Angew. Chem., Int. Ed.* **2015**, *54*, 2151−2155.
(27) Wu, N.; Wang, K.; Wang, Y.-T.; Chen, M.-L.; Chen, X.-W.; Yang, T.; Wang, J.-H. *Anal. Chem.* **2020**, *92*, 11111−11118.

(28) Chen, K.; Huang, Q.; Fu, T.; Ke, G.; Zhao, Z.; Zhang, X.; Tan, W. *Anal. Chem.* **2020**, *92*, 7404−7408.
(29) Zhang, H.; Xu, X.; Jiang, W. *Chem. Sci.* **2020**, *11*, 7415−7423.
(30) Zheng, J.; Li, N.; Li, C.; Wang, X.; Liu, Y.; Mao, G.; Ji, X.; He, Z. *Biosens. Bioelectron.* **2018**, *107*, 40−46.
(31) Lv, H.; Chen, A.; Cheng, W.; Kong, L.; Zhao, M.; Ding, S.; Ju, H.; Cheng, W. *Anal. Chem.* **2020**, *92*, 15624−15631.
(32) Zhou, H.; Duan, S.; Huang, J.; He, F. *Chem. Commun.* **2020**, *56*, 6273−6276.
(33) Man, Y.; Liu, J.; Wu, J.; Yin, L.; Pei, H.; Wu, Q.; Xia, Q.; Ju, H. *Anal. Chim. Acta* **2020**, *1107*, 48−54.
(34) Jung, C.; Allen, P. B.; Ellington, A. D. *ACS Nano* **2017**, *11*, 8047−8054.
(35) Zhong, X.; Yang, S.-S.; Liao, N.; Yuan, R.; Zhuo, Y. *Anal. Chem.* **2021**, *93*, 5301−5308.
(36) Wang, Q.; Wen, Y.; Li, Y.; Liang, W.; Li, W.; Li, Y.; Wu, J.; Zhu, H.; Zhao, K.; Zhang, J.; Jia, N.; Deng, W.; Liu, G. *Anal. Chem.* **2019**, *91*, 9277−9283.
(37) Pei, H.; Li, F.; Wan, Y.; Wei, M.; Liu, H.; Su, Y.; Chen, N.; Huang, Q.; Fan, C. *J. Am. Chem. Soc.* **2012**, *134*, 11876−11879.
(38) Huang, C.; Liu, Y.; Sun, Y.; Wang, F.; Ge, S.; Yu, J. *ACS Appl. Mater. Interfaces* **2021**, *13*, 35389−35396.
(39) Zhong, W.; Wu, J.; Huang, Y.; Xing, C.; Lu, C. *Langmuir* **2022**, *38*, 1151−1157.
(40) Cheng, X.; Bao, Y.; Liang, S.; Li, B.; Liu, Y.; Wu, H.; Ma, X.; Chu, Y.; Shao, Y.; Meng, Q.; Zhou, G.; Song, Q.; Zou, B. *Anal. Chem.* **2021**, *93*, 9593−9601.
(41) Zhang, X.; Wei, X.; Qi, J.; Shen, J.; Xu, J.; Gong, G.; Wei, Y.; Yang, J.; Zhu, Q.; Bai, T.; Guo, Z.; Qu, X.; Zhu, Y. *Anal. Chem.* **2022**, *94*, 4787−4793.
(42) Chai, H.; Miao, P. *Anal. Chem.* **2019**, *91*, 4953−4957.
(43) Wang, C.; Song, H.; Zhao, X.; Liu, R.; Lv, Y. *Anal. Chem.* **2022**, *94*, 1787−1794.
(44) Du, M.; Zheng, J.; Tian, S.; Liu, Y.; Zheng, Z.; Wang, H.; Xia, J.; Ji, X.; He, Z. *Anal. Chem.* **2021**, *93*, 5606−5611.
(45) Wang, Q.; Liu, Y.; Yan, J.; Liu, Y.; Gao, C.; Ge, S.; Yu, J. *Anal. Chem.* **2021**, *93*, 13373−13381.
(46) Li, L.; Zhang, Y.; Yan, Z.; Chen, M.; Zhang, L.; Zhao, P.; Yu, J. *ACS Sens.* **2020**, *5*, 1482−1490.
(47) Gao, Y.; Zhang, S.; Wu, C.; Li, Q.; Shen, Z.; Lu, Y.; Wu, Z.-S. *ACS Nano* **2021**, *15*, 19211−19224.
(48) Yang, Z.; Peng, X.; Yang, P.; Zhuo, Y.; Chai, Y.-Q.; Liang, W.; Yuan, R. *Chem. Sci.* **2020**, *11*, 8482−8488.
(49) Yang, J.; Li, Y.; Guo, L.; Qiu, B.; Lin, Z. *Anal. Chem.* **2021**, *93*, 11010−11018.
(50) Niu, X.; Lu, C.; Su, D.; Wang, F.; Tan, W.; Qu, F. *Anal. Chem.* **2021**, *93*, 13727−13733.
(51) Wang, Q.; Liu, Y.; Yan, J.; Liu, Y.; Gao, C.; Ge, S.; Yu, J. *Anal. Chem.* **2021**, *93*, 13373−13381.
(52) Song, Z.; Ma, Y.; Chen, M.; Ambrosi, A.; Ding, C.; Luo, X. *Anal. Chem.* **2021**, *93*, 5963−5971.
(53) Zhou, H.; Zhang, J.; Li, B.; Liu, J.; Xu, J.-J.; Chen, H.-Y. *Anal. Chem.* **2021**, *93*, 6120−6127.
(54) Mensah, K.; Cissé, I.; Pierret, A.; Rosticher, M.; Palomo, J.; Morfin, P.; Plaçais, B.; Bockelmann, U. *Adv. Healthcare Mater.* **2020**, *9*, 2000260.
(55) Guo, Q.; Yu, Y.; Zhang, H.; Cai, C.; Shen, Q. *Anal. Chem.* **2020**, *92*, 5302−5310.
(56) Zhang, X.; Yang, Z.; Chang, Y.; Qing, M.; Yuan, R.; Chai, Y. *Anal. Chem.* **2018**, *90*, 9538−9544.
(57) Wei, J.; Wang, H.; Wu, Q.; Gong, X.; Ma, K.; Liu, X.; Wang, F. *Angew. Chem., Int. Ed.* **2020**, *59*, 5965−5971.

https://doi.org/10.1021/acs.analchem.2c02004
Anal. Chem. 2022, 94, 10524−10530